Shell model study of $^{40}S(\beta^-)^{40}Cl$ and the energy levels of ^{40}Cl

E. K. Warburton
Brookhaven National Laboratory, Upton, New York 11973
and Max-Planck-Institut für Kernphysik, D-6900 Heidelberg, Federal Republic of Germany

J. A. Becker
Lawrence Livermore National Laboratory, Livermore, California 94550
(Received 19 December 1988)

Shell-model calculations are performed for the odd- and even-parity states of ^{40}Cl and the 0^+ ^{40}S ground state. The ^{40}Cl odd-parity states and the ^{40}S 0^+ levels were considered in full $(2s,1d)^{21}(1f,2p)^3$ and $(2s,1d)^{20}(1f,2p)^4$ configurational spaces, respectively. For the ^{40}Cl even-parity states it was necessary to use a highly truncated $(2s,1d)^{20}(1f,2p)^4$ configurational space. Besides energy spectra and binding energies, observables calculated are first-forbidden and allowed β^- decay of ^{40}S, γ transitions in ^{40}Cl, and one-body density overlaps of the odd-parity states of ^{40}Cl with the ^{40}Ar ground state. The results are compared to experiment. For example, the half-life of ^{40}S is predicted to be in the range 6.2–16.6 s (depending on the assumed level scheme) as compared to the experimental value of 8.8 ± 2.2 s.

I. INTRODUCTION

The shell-model predictions presented here for the β^- decay of ^{40}S and the spectroscopy of ^{40}Cl are a continuation of an investigation into the structure of neutron-rich $A\sim40$ nuclei.[1–8] This study utilizes a spherical harmonic oscillator basis and a shell-model interaction—designated WBMB—designed to describe nuclear levels in the $A\sim40$ region for which the nucleons occupy the seven subshells of the (sd) and (fp) major shells. Hamiltonian diagonalization is carried out in the $(2s,1d)^{A-16-n}(1f,2p)^n$ model space for a single value of n. Our shorthand for this model space is nfp.

There have been no previously reported shell-model calculations for ^{40}S. Calculations for ^{40}Cl have been reported by Woods[9] and by Ji and Wildenthal.[10] Woods used a model space of $(d_{3/2},s_{1/2})^9$, $(f_{7/2},p_{3/2})^3$; i.e., the $sdpf$ space was truncated by omitting the $d_{5/2}$, $f_{5/2}$, and $p_{1/2}$ orbits. As discussed in Sec. III, our calculations indicate that this truncation is quite valid for the calculation of the ^{40}Cl odd-parity energy spectrum which was all that Woods considered. Ji and Wildenthal used a model space of $d_{3/2}^{-3-n}f_{7/2}^{3+n}$; $n=0,2,4$. Thus the allowable orbits are drastically curtailed but, unlike the present calculations or those of Woods,[9] 2p-2h and 4p-4h excitations are allowed. Again, only the energy spectrum was considered. From our point of view, the chief value of the Ji-Wildenthal[10] calculation is in indicating that the low-lying odd-parity states are $\sim80\%$ $0\hbar\omega$. This is representative of the nuclei we have considered with the WBMB interaction so that our neglect of $n\hbar\omega$ excitations is presumably compensated by our effective interaction and the use of effective operators.

Dufour, *et al.*[11] have reported the observation of β^--delayed γ ray spectra from the decay of twelve neutron-rich nuclei. The research was conducted at GANIL (Grand Accéléreteur National d'Ions Lourds, Caën, France). Of these decaying nuclei, seven have $N>20$, $Z<20$ and thus involve both the (sd) and (fp) shells. We have previously reported calculations for the five with $N=21$ and 22 utilizing $1fp$ and $2fp$ model spaces.[2,5] Here we consider the $N=24$ nucleus ^{40}S for which the $4fp$ model space is appropriate. It will decay by allowed β^- transitions to $4fp$ states of ^{40}Cl and by first-forbidden β^- transitions to $3fp$ states. We will consider both of these types of decay.

^{40}Cl itself decays by β^- emission to ^{40}Ar (Refs. 12 and 13) and the decay modes establish the ^{40}Cl ground state as 2^-. In addition to beta decay, information on the energy levels of ^{40}Cl has been deduced from the $^{40}Ar(^7Li,^7Be)^{40}Cl$ (Ref. 14) and $^9Be(^{36}S,\alpha p\gamma)^{40}Cl$ (Ref. 15) reactions. We shall consider aspects of both studies.

II. THE CALCULATION

The WBMB interaction for the $sdpf$ model space is derived from an effective one-body plus two-body Hamiltonian and is composed of three parts. The starting point is the "universal" $(2s,1d)$ interaction, denoted USD, of Wildenthal.[16] Interactions between $(1f,2p)$ nucleons are accounted for by an interaction developed by McGrory[17] and the cross shell interaction connecting the $(2s,1d)$ and $(1f,2p)$ shells was generated from the nucleon-nucleon potential of the Millener-Kurath interaction.[18] The relative single-particle energies of the three sd shell orbits and the four fp shell orbits were taken from the USD and McGrory interactions, respectively. The energy gap between the sd and fp shells was determined from a consideration of binding energies of $A=35$–43 nuclei.[4] The calculation is performed with[19] OXBASH using an isospin formalism. Details of calculations using OXBASH with the WBMB interaction have been given previously.[4–8]

Our disc-space resources allow us to diagonalize J-

matrices up to a dimension, $D(J)$, of about 6000 depending on the m dimension, $D(m)$. In our *sdpf* model space the odd-parity states of ^{40}Cl have a maximum $D(J)$ of 4217 at $J^\pi=3^-$ and therefore truncation was not required for these states. The $D(J)$ and $D(m)$ for the ^{40}S 0^+ states are 6351 and 230 025 which is very near our present capabilities. At the time this work was commenced some truncation was necessary but eventually diagonalization was achieved in the full *sdpf* model space. We present aspects of both results in order to indicate the effects of truncation. Unless otherwise stated, results involving the ^{40}S ground state are for the untruncated calculation.

In OXBASH, truncation can be accomplished by selection of partitions; a partition being a specific occupancy of the subshells included in the interaction. We designate the partitions as

$$[\mathbf{n(d_{5/2}),n(d_{3/2}),n(s_{1/2});n(f_{7/2}),n(f_{5/2}),n(p_{3/2}),n(p_{1/2})}] \quad (1)$$

where $n(j)$ is the occupancy of the subshell j. Once the necessary degree of truncation is determined, the optimum truncation scheme depends on the observables to be calculated. Our truncated calculation for ^{40}S was done with the following set of partitions from the unrestricted complement of 372:

[8-12,4-8,2-4;0-4,0-2,0-4,0-2],

which, for $T_z=4$, consists of four unrestricted proton holes in the *sd* shell and four neutrons in the *fp* shell with occupancy of the $f_{5/2}$ orbit restricted to at most two neutrons. The $D(J)$ for the 324 partitions of this truncation is 3984.

The $D(J)$ are roughly an order of magnitude too large for the even-parity states of ^{40}Cl and a severe truncation is necessary. That chosen is the 24 partitions of the four following sets:

[12,8-r,r;3-4,0-1,0-1,0-1]r=1-4 ,

[12,8-r,r;2,0,2,0]r=1-4 ,

[11,5,4;3-4,0,0-1,0-1] ,

[11,5,4;2,0,2,0] .

In the first two of these, e.g., ^{32}S is a closed core. For this truncation, the $D(J)$ for the ^{40}Cl 1^+ states is 2206; and $D(J)$ reaches a maximum of 4266 for $J^\pi=4^+$. Calculations for the $3fp$ states of ^{40}Cl and the $4fp$ states of ^{40}S in the full *sdpf* model space are free of spuriosity. In the other cases, spuriosity is routinely eliminated by the *approximate* method of Gloeckner and Lawson.[20]

III. RESULTS

A. Wave functions, spectra, and binding energies

The compositions of the ^{40}Cl 2_1^- and 5_1^- states are shown in Table I, and the compositions of the ^{40}S 0_1^+ and ^{40}Cl 1_1^+ states are considered in Table II. We first consider the odd-parity levels. As expected, the largest component in the yrast $J=2-5$ states is $(d_{3/2}^{-3})(f_{7/2}^{3})$. The percentages are 55, 47, 61, and 63, respectively. The 1_1^- state is also mainly $(d_{3/2}^{-3})(f_{7/2}^{3})$, 43%. The 0_1^- state is

TABLE I. Composition of the 2_1^- and 5_1^- ^{40}Cl wave functions. Only those partitions are listed which have contributions of $>1\%$ to either state. The three lines at the bottom give the total contribution of the energy unfavored orbits.

Partition	Configuration	Intensity (in %) ^{40}Cl 2_1^-	Intensity (in %) ^{40}Cl 5_1^-
[12,5,4;3,0,0,0]	$(d_{3/2}^{-3})(f_{7/2}^{3})$	54.61	63.42
[12,6,3;3,0,0,0]	$(d_{3/2}^{-2}s_{1/2}^{-1})(f_{7/2}^{3})$	11.40	7.50
[11,7,3;3,0,0,0]	$(d_{5/2}^{-1}d_{3/2}^{-1}s_{1/2}^{-1})(f_{7/2}^{3})$	1.58	1.58
[12,7,2;3,0,0,0]	$(d_{3/2}^{-1}s_{1/2}^{-2})(f_{7/2}^{3})$	0.91	1.99
[11,6,4;3,0,0,0]	$(d_{5/2}^{-1}d_{3/2}^{-2})(f_{7/2}^{3})$	2.16	2.92
[10,7,4;3,0,0,0]	$(d_{5/2}^{-2}d_{3/2}^{-1})(f_{7/2}^{3})$	2.20	2.71
[12,6,3;2,0,1,0]	$(d_{3/2}^{-2}s_{1/2}^{-1})(f_{7/2}^{2}p_{3/2}^{1})$	7.10	2.90
[12,5,4;2,0,1,0]	$(d_{3/2}^{-3})(f_{7/2}^{2}p_{3/2}^{1})$	5.60	2.01
[12,5,4;2,1,0,0]	$(d_{3/2}^{-3})(f_{7/2}^{2}f_{5/2}^{1})$	1.20	1.56
[12,5,4;1,0,2,0]	$(d_{3/2}^{-3})(f_{7/2}^{1}p_{3/2}^{2})$	4.28	5.33
[12,5,4;1,2,0,0]	$(d_{3/2}^{-3})(f_{7/2}^{1}f_{5/2}^{2})$	1.86	2.57
[12,5,4;1,0,0,2]	$(d_{3/2}^{-3})(f_{7/2}^{1}p_{1/2}^{2})$	0.81	1.19
Sum		93.61	95.68
Contribution of $p_{1/2}$ orbit to wave function		2.27	1.88
Contribution of $f_{5/2}$ orbit to wave function		5.43	6.26
Contribution of $n(d_{5/2})<12$ to wave function		8.72	9.30

TABLE II. Composition of the 0_1^+ ^{40}S and 1_1^+ ^{40}Cl wave functions. Only those partitions are listed which have contributions of $>2\%$ to either state. The three lines at the bottom give the total contribution of the energy unfavored orbits to the ^{40}S 0_1^+ state.

Partition	Configuration	Intensity (in %) ^{40}S 0_1^+	Intensity (in %) ^{40}Cl 1_1^+
[12,4,4;4,0,0,0]	$(d_{3/2}^{-4})(f_{7/2}^{4})$	26.83	26.07
[12,6,2;4,0,0,0]	$(d_{3/2}^{-2}s_{1/2}^{-2})(f_{7/2}^{4})$	16.20	2.67
[12,5,3;4,0,0,0]	$(d_{3/2}^{-3}s_{1/2}^{-1})(f_{7/2}^{4})$	7.18	36.51
[11,5,4;4,0,0,0]	$(d_{5/2}^{-1}d_{3/2}^{-3})(f_{7/2}^{4})$	1.40	5.62
[10,6,4;4,0,0,0]	$(d_{5/2}^{-2}d_{3/2}^{-2})(f_{7/2}^{4})$	3.44	a
[12,4,4;2,0,2,0]	$(d_{3/2}^{-4})(f_{7/2}^{2}p_{3/2}^{2})$	8.30	2.05
[12,5,3;2,0,2,0]	$(d_{3/2}^{-3}s_{1/2}^{-1})(f_{7/2}^{2}p_{3/2}^{2})$	1.00	2.59
[12,6,2;2,0,2,0]	$(d_{3/2}^{-2}s_{1/2}^{-2})(f_{7/2}^{2}p_{3/2}^{2})$	2.60	0.14
[12,5,3;3,0,1,0]	$(d_{3/2}^{-3}s_{1/2}^{-1})(f_{7/2}^{3}p_{3/2}^{1})$	7.71	6.94
[12,4,4;3,0,1,0]	$(d_{3/2}^{-4})(f_{7/2}^{3}p_{3/2}^{1})$	0.96	11.18
[12,6,2;3,0,1,0]	$(d_{3/2}^{-2}s_{1/2}^{-2})(f_{7/2}^{3}p_{3/2}^{1})$	2.34	0.68
[12,4,4;2,2,0,0]	$(d_{3/2}^{-4})(f_{7/2}^{2}f_{5/2}^{2})$	2.81	a
Sum		80.76	94.45
Contribution of $p_{1/2}$ orbit to wave function		3.86	
Contribution of $f_{5/2}$ orbit to wave function		10.21	
Contribution of $n(d_{5/2})<12$ to wave function		13.18	

[a]Not included in the model space.

66% $(d_{3/2}^{-3})(f_{7/2}^{2}p_{3/2}^{1})$. In general, the results of Table I are representative of the 3_1^- and 4_1^- states as well. It is seen that the wave functions are relatively simple in the sense that only twelve of the allowable 200 partitions comprise $>93\%$ of the wave functions.

In contrast, the wave function of the ^{40}S ground state is considerably more complex. The twelve partitions listed in Table II make up 81% of the wave function, the remaining 19% is spread over many partitions which individually contribute $<2\%$. Other than that, there are no surprises except, perhaps, for the large contributions from $d_{5/2}^{-2}$ and $f_{5/2}^{2}$.

A common truncation of the *sdpf* space in this region of A is to the valence orbitals $(s_{1/2},d_{3/2},f_{7/2},p_{3/2})$, e.g., see Ref. 9. The rather small contributions of the $d_{5/2}$, $f_{5/2}$, and $p_{1/2}$ orbits to the wave functions of the yrast odd-parity states of ^{40}Cl and the 0_1^+ ^{40}S state supports the validity of this truncation, at least for observables which are not sensitive to the presence of spin-orbit partners and if spuriosity is not a problem.

The experimental binding energies of ^{40}S and ^{40}Cl are 332 860(40) keV (Ref. 21) and 337 082(35) keV (Ref. 14), respectively. The $^{40}S(\beta^-)^{40}Cl$ Q value calculated from the experimental binding energies is 5004(53) keV. The WBMB interaction has good predictive powers for binding energies. For fourteen $N=21$ and 22 nuclei in the $A=35-42$ region, the mean deviation from experimental binding energies is 236 keV.[4] The WBMB prediction for the 2^- ^{40}Cl ground-state binding energy is 337 228 keV: 146(35) keV more bound than experiment. The calculated binding energy of ^{40}S is 332 746 keV: 114 keV less bound than experiment. For the truncated model space the calculated binding energy was 332 646 keV: only 100 keV less bound than for the full model space. The omission of the 48 partitions with $n(f_{5/2})=3,4$ is seen to have little effect on the calculated energy. (Note that the effect of truncation on a ground state is always to make it less bound.) This is not surprising since the omitted partitions were found to contribute only 0.11% to the ground-state wave function in the untruncated calculation. The truncation also had negligible effect on the β^- decay rates to be described in the next subsection.

Since the calculations for the positive-parity states of ^{40}Cl were, of necessity, carried out in a highly truncated basis, meaningful absolute binding energies for these states were not obtained. The decay schemes constructed from the $^{40}S(\beta^-)^{40}Cl$ results of Dufour *et al.*[11] (Sec. IV) imply an even-parity spectrum commencing some 0.5–1.0 MeV above the ^{40}Cl ground state. To accommodate this, we need to lower our calculated even-parity excitation energies by $\sim 4.0-3.5$ MeV. From our previous experience with truncation within the *sdpf* model space, this seems reasonable for the truncation used. The predicted odd- and even-parity spectra of ^{40}Cl are listed in Table III. We will compare these predictions to experiment in Sec. IV.

B. Beta and gamma decays

1. First forbidden beta decay

We first consider the first-forbidden β^- decay of ^{40}S to the odd-parity ^{40}Cl states. The calculations were carried

out with the effective operators described in Ref. 7. Using the ^{40}S half-life of 8.8(22) s (Ref. 11), we calculate a total first-forbidden branching ratio of 0.94% with the only branches greater than 0.01% proceeding to the 0_1^-, 0_2^-, 1_1^-, and 2_1^- states, respectively. The predictions for these four states are given in Table IV. The unique decay to 2_1^- falls within the range of normal strengths. It is 22% of a single-particle $f_{7/2}\leftrightarrow d_{3/2}$ transition, i.e., a unique single-particle $0^+\rightarrow 2^-$ decay rate reduced by a factor of 3.8 (which is the average quenching for this region[7]). The $0^+\rightarrow 0^-$ decays are considerable weaker. They are 1.3% and 5.3% of an $A=40$ $d_{3/2}\leftrightarrow p_{3/2}$ single-particle estimate (see Table II of Ref. 7). The weakness of the total first-forbidden branching is due to the relative smallness of these matrix elements and to the rather low energy release for such a neutron-rich decay, i.e., ^{40}S is quite tightly bound. At the present stage of experimental knowledge, these first-forbidden branches are completely

TABLE III. The odd-parity ($3fp$) and even-parity ($4fp$) spectra of ^{40}Cl calculated with the WBMB interaction. The odd-parity spectrum was generated from the full *sdpf* model space. The even-parity spectrum was generated from a truncated model space as discussed in the text. All states are shown up to 4_8^- (for $3fp$) and 2_8^+ (for $4fp$), after that only yrast states are listed.

	$3fp$			$4fp$	
E_x (keV)	J^π	No.	E_x (keV)	J^π	No.
0	2^-	1	0	2^+	1
133	3^-	1	153	1^+	1
253	1^-	1	440	3^+	1
382	4^-	1	516	2^+	2
515	2^-	2	573	0^+	1
740	4^-	2	995	3^+	2
835	5^-	1	1022	1^+	2
855	3^-	2	1049	4^+	1
1001	3^-	3	1266	4^+	2
1078	0^-	1	1272	0^+	2
1197	3^-	4	1281	2^+	3
1205	1^-	2	1404	2^+	4
1490	2^-	3	1457	5^+	1
1528	1^-	3	1534	2^+	5
1550	4^-	3	1561	3^+	3
1831	3^-	5	1723	2^+	6
1869	2^-	4	1733	4^+	3
2010	3^-	6	1743	1^+	3
2037	0^-	2	1801	3^+	4
2069	2^-	5	1905	6^+	1
2215	4^-	4	1919	4^+	4
2237	2^-	6	1929	1^+	4
2325	6^-	1	1965	3^+	5
2352	1^-	4	1966	5^+	2
2387	2^-	7	2052	6^+	2
2450	5^-	2	2057	2^+	7
2614	4^-	5	2079	4^+	5
2729	2^-	8	2101	3^+	6
2750	3^-	7	2117	5^+	3
2826	4^-	6	2126	4^+	6
2838	1^-	5	2151	3^+	7
2844	5^-	3	2155	6^+	3
2846	3^-	8	2169	1^+	5
2861	7^-	1	2235	2^+	8
2895	4^-	7	2499	7^+	1
2944	4^-	8	3285	8^+	1
4291	8^-	1	4130	9^+	1
4354	9^-	1	5357	10^+	1
7150	10^-	1	5819	11^+	1
11 108	11^-	1	7421	12^+	1
11 957	12^-	1	8706	13^+	1
16 439	13^-	1	11 710	14^+	1
23 296	14^-	1	13 271	15^+	1

TABLE IV. First-forbidden beta decay of ^{40}S to states of ^{40}Cl. The results shown are the four decays with β^- branching ratios calculated to be greater than 0.01%.

^{40}Cl state	Q (MeV)[a]	f[b]	log f_0t	BR (%)[c]
0_1^-	3.925	1.73	6.93	0.25
0_2^-	2.966	1.98	6.34	0.28
1_1^-	4.793	0.23	8.21	0.03
2_1^-	5.004	2.41	7.27	0.34

[a]The 1_1^- and 2_1^- Q values are experimental (see Sec. IV); the 0^- Q values are calculated from the excitation energies of Table III.
[b]$\tau^{-1}(\text{sec}^{-1}) = \ln 2/t_{1/2} = f/8896$; ft = 6166 sec.
[c]β^- branching ratio.

negligible so that ^{40}S β^- decay can be considered as proceeding to 1^+ states alone.

2. *Allowed beta decay*

For the Gamow-Teller (GT) operator—and the similar $M1$ electromagnetic operator—Brown and Wildenthal[22,23] extracted effective operators for the *sd* shell from a least-squares fit to empirical GT and $M1$ matrix elements. We use their results for the *sd* shell. For the *fp* shell we use the fundamental results of Towner[24] modified to reproduce exactly the experimental $^{41}Sc(\beta^+)^{41}Ca$ GT matrix element and the ^{41}Ca and ^{41}Sc magnetic moments as explained in Ref. 8.

Gamow-Teller matrix elements were calculated for the decay of the 0^+ ^{40}S ground state to all energetically accessible ^{40}Cl 1^+ states. The total needed was ~ 50; the exact number depends on the increment of excitation energy added to the even-parity spectrum of Table III as will be discussed in Sec. IV. Predictions for the Gamow-Teller beta strength, B(GT), and log f_0t-values for the first fifteen 1^+ states of ^{40}Cl are listed in Table V. These results will be compared to experiment in the next section (Sec. IV B).

3. *Gamma decay*

Our calculations of electromagnetic matrix elements were confined to $M1$ and $E2$ decays between the low-lying odd-parity levels of ^{40}Cl. Decays involving the even-parity levels of ^{40}Cl were not considered for two reasons: (1) Our previous experience[4] has shown that the WBMB model space is inadequate for the calculation of $E1$ rates in the $A \sim 40$ region, and (2) the truncation of the $4fp$ model space is severe enough so that any predictions of individual electromagnetic transition rates involving these states would be of doubtful value. The effective $M1$ operator used was described in the last subsection (Sec. III B 2). For $E2$ transitions we use $e_p = 1.29e$, $e_n = 0.49e$, as discussed previously,[4,8] and an oscillator parameter of 1.9623 fm. Results pertinent to the present study are collected in Table VI.

TABLE V. Predictions for the allowed β^- decay of ^{40}S to 1^+ states of ^{40}Cl. The ^{40}Cl excitation energy, E_x, is that of Table III. The B(GT) values are calculated with the effective operator described in the text. Log f_0t is defined as $\log_{10}[6166/B(\text{GT})]$. The 15 decays shown represent > 99% of the total GT branching.

Number of state	E_x (keV)[a]	B(GT) ($\times 10^3$)	log f_0t
1	153	17.3	5.55
2	1022	94.4	4.82
3	1743	7.3	5.93
4	1929	600.7	4.01
5	2169	98.8	4.80
6	2307	63.0	4.99
7	2442	84.6	4.86
8	2523	5.4	5.06
9	2652	27.1	5.36
10	2780	49.5	5.10
11	2871	306.5	4.30
12	3078	1.2	6.72
13	3125	8.9	5.84
14	3232	3.8	6.21
15	3318	24.4	5.40

[a]Relative energies, see Table III and the text.

TABLE VI. $B(M1)$ and $B(E2)$ values for transitions between the low-lying, odd-parity states of ^{40}Cl. The $B(M1)$ and $B(E2)$ are in Weisskopf units (W.U.).

J_i^π	J_f^π	$B(M1)$	$B(E2)$
1_1^-	2_1^-	1.8×10^{-3}	6.91
3_1^-	1_1^-		1.56
3_1^-	2_1^-	95.5×10^{-3}	1.17
4_1^-	2_1^-		1.99
4_1^-	3_1^-	6.8×10^{-3}	0.33
5_1^-	3_1^-		3.45
5_1^-	4_1^-	91.1×10^{-3}	3.86

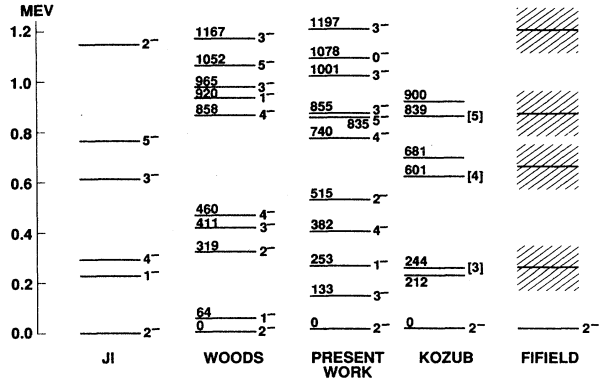

FIG. 1. Comparison of theoretical and experimental level schemes for ^{40}Cl

IV. COMPARISON TO EXPERIMENT

A. The odd-parity levels of ^{40}Cl

The experimental ^{40}Cl level schemes of Fifeld, *et al.*[14] and of Kozub, *et al.*[15] are compared to the present $3fp$ predictions and those of Woods[9] and Ji and Wildenthal[10] in Fig. 1. The energy resolution of 180 keV in the ^{40}Ar(^{7}Li,^{7}Be)^{40}Cl experiment is indicated by cross hatching in order to show clearly that the two experimental schemes are consistent. The speculative spin assignments of Kozub, *et al.* arise from consideration of the reaction mechanism of heavy-ion fusion-evaporation reactions—such as the ^{9}Be+^{36}S$\rightarrow^{45}$Ca$\rightarrow^{40}$Cl+α+p+γ reaction in question—and from relative angular intensities observed in γ ray coincidences. Although these assignments are not definite, the heavy-ion fusion-evaporation mechanism is so well understood and so selective of yrast states that these spin assignments can be assigned a high probability. It was implicitly assumed in previous studies[10,15] that the levels observed by Kozub, *et al.* have odd parity although the ^{36}S+^{9}Be results give no parity preference. As discussed in the next subsection (Sec. IV B), our placement of the $4fp$ even-parity states relative to the odd-parity states supports this view, and we too make the assumption (model dependent) that the levels observed by Kozub, *et al.* have odd parity. That is, the heavy-ion fusion-evaporation reaction is selective of yrast states and our predictions are that the low-lying yrast states have odd parity. We also assume—on the basis of the model predictions of Fig. 1—that the 212-keV level is the 1_1^- state. The relative cross section for populating ^{40}Cl levels via the (^{7}Li,^{7}Be) reaction has been the subject of previous speculation and we next consider this question in some detail.

1. ^{40}Ar$\rightarrow^{40}$Cl charge exchange

It seems reasonable to assume—as in previous studies[14,15,10]—that the ^{40}Ar(^{7}Li,^{7}Be)^{40}Cl reaction proceeds predominantly by a one-step charge-exchange mechanism, i.e., $\pi(sd)\rightarrow\nu(fp)$. In general, there will be numerous operators contributing to the reaction and a viable, quantitative study of the reaction mechanism would be a formidable task. However, some qualitative understanding can be had from a consideration of the one-body-density-matrix-elements (OBDME) for the assumed process. Schematically,

$$[\sigma_{ce}(\Theta)]^{1/2}=\sum_{j_i,j_f}\Xi(j_i,j_f;\Theta)\langle J_fT_f|||(a_{j_f}^\dagger\tilde{a}_{j_i})^{\Delta J\Delta T}|||J_iT_i\rangle \quad (2)$$

where $\sigma_{ce}(\Theta)$ is the reaction cross section at angle Θ, and ΔJ and ΔT are the space-spin and isospin ranks of the

TABLE VII. One-body-density-matrix elements (OBDME) for a one-step $\pi(sd)\rightarrow\nu(fp)$ charge exchange between the ^{40}Ar ground state and the 2_1^-, 3_1^-, 4_1^-, and 5_1^- levels of ^{40}Cl. The normalization is such that the OBDME for a single-particle transition is unity.

j_i	j_f	2_1^-	3_1^-	4_1^-	5_1^-
$d_{5/2}$	$f_{7/2}$	−0.001 66	−0.073 52	−0.080 63	−0.016 31
$d_{3/2}$	$f_{7/2}$	+0.669 32	+0.711 04	+0.851 99	−0.803 14
$s_{1/2}$	$f_{7/2}$		−0.401 59	+0.148 41	
$d_{5/2}$	$f_{5/2}$	+0.052 64	−0.000 82	+0.034 65	−0.007 19
$d_{3/2}$	$f_{5/2}$	+0.077 31	+0.036 51	−0.126 96	
$s_{1/2}$	$f_{5/2}$	+0.040 38	−0.071 30		
$d_{5/2}$	$p_{3/2}$	+0.016 44	+0.044 65	+0.018 50	
$d_{3/2}$	$p_{3/2}$	+0.199 66	+0.197 53		
$s_{1/2}$	$p_{3/2}$	+0.206 89			
$d_{5/2}$	$p_{1/2}$	+0.019 67	−0.000 71		
$d_{3/2}$	$p_{1/2}$	−0.020 67			

operators α, i.e.,

$$\Xi(j_i,j_f;\Theta)=\sum_{\alpha}\Xi(j_i,j_f;\Theta,\alpha) \quad (3)$$

contains all the information on the reaction mechanism and is a sum over terms (schematic) representing all the possible operators. We are mainly concerned here with the OBDME—represented by the last term in Eq. (2). These define the dependence of the reaction on the wave functions of ^{40}Ar and ^{40}Cl. Our results for the 2_1^-, 3_1^-, 4_1^-, and 5_1^- states of ^{40}Cl are given in Table VII. It was speculated in previous studies[14,9] that these four yrast states arise from the weak coupling $(^{37}\text{Cl;g.s.})_{3/2^+}\otimes(^{43}\text{Ca;g.s.})_{7/2^-}$ and supply the dominant charge-exchange cross sections to the low energy region of ^{40}Cl. It was also assumed that the $\frac{3}{2}^+$ and $\frac{7}{2}^-$ wave functions are composed of simple $d_{3/2}f_{7/2}$ components. We find the situation to be more complicated. As shown in Table VII, the $\pi(d_{3/2})\rightarrow\nu(f_{7/2})$ OBDME has the largest amplitude as expected; however for 2_1^- and 3_1^- other $j_i\rightarrow j_f$ transitions are hardly negligible. Consider, for example the equivalent operator to unique, first-forbidden beta decay ($\Delta J=2$, $\Delta\pi=-$). It is important to note that it vanishes for odd J, odd parity ^{40}Cl states and thus is identically zero for the 3^- and 5^- levels while for the 2_1^- level, for example, the ten contributing $j_i\rightarrow j_f$ transitions add destructively so that the resulting matrix element is 56% of a pure $d_{3/2}\rightarrow f_{7/2}$ one. This example is given to illustrate the possibilities; for any specific operator, selection rules can forbid some transitions and the physics may quench or enhance others. Since there are other operators contributing to the charge exchange, the situation is complex. A few general remarks can be made as follows.

(1) With our assumptions, the OBDME for the $2fp$ ^{40}Ar ground state connecting to $4fp$ even-parity states of ^{40}Cl are zero.

(2) The OBDME for 1_1^- and 6_1^- are all small while that for the 0_1^- has a large dominant $d_{3/2}\rightarrow p_{3/2}$ contribution.

(3) The OBDME for the first five 2^- and 3^- levels all have complex compositions with several large terms contributing to each state.

(4) There are large OBDME for the second and third 4^- levels.

(5) All OBMDE are small for the second thru fifth 5^- states.

From this summary we can conclude that the charge exchange cross sections for the 1_1^- and 6_1^- states and the higher 5^- states are predicted to be small. Other than that, the relative cross sections will depend very much on the strengths and natures of the contributing operators and cannot be *a priori* predicted from the OBDME.

2. *Gamma-ray transitions*

At present, the only pertinent comparison of the $B(M1)$ and $B(E2)$ predictions of Table VI to experiment is for the branching ratios of the 4_1^- and 5_1^- levels. The main decay mode observed by Kozub, *et al.* was $839\rightarrow601\rightarrow244\rightarrow0$ and the experiment gave most probable $J_i=J_f+1$ assignments for each transition; hence the most probable spins of Fig. 1. Assuming the spins postulated by Kozub, *et al.* (Fig. 1), the $B(M1)$ and $B(E2)$ values of Table VI give a competing $E2$ $4_1^-\rightarrow2_1^-$ branch of 14% in nice agreement with the experimental value of 11(4)% (Ref. 15). Likewise, the competing $E2$ $5_1^-\rightarrow3_1^-$ branch is predicted to be 7%. A $839[5^-]\rightarrow244[3^-]$ transition was not observed by Kozub, *et al.*; however, the predicted branch is weak enough so that it would most probably have been overlooked.[25]

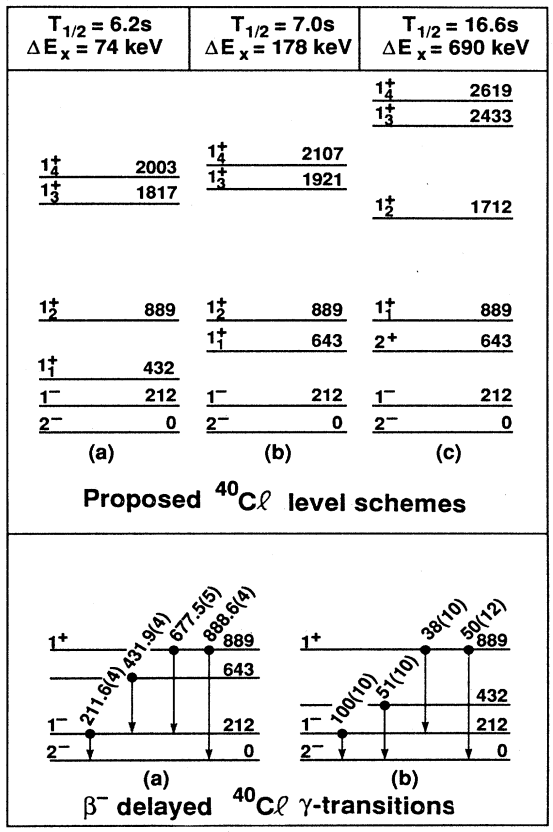

FIG. 2. Proposed level schemes for ^{40}Cl from $^{40}S(\beta^-)^{40}Cl$. Lower panel: The two most likely placements of the four β^--delayed γ-transitions in ^{40}Cl observed by Dufour, *et al.* (Ref. 11). The γ-ray energies (in keV) are shown in (a) and the relative intensities in (b). The schemes (a) and (b) differ only in the placement of the 432-keV transition. The evidence for the spin-parity assignments is discussed in the text. Upper panel: Three possible placements of the even-parity spectrum of ^{40}Cl relative to the odd-parity spectrum. In all three cases the two lowest even-parity levels are placed as in (a) or (b) of the lower panel and ΔE_x is defined as the difference between the average experimental excitation energy for the two levels and the average excitation energy of the two levels in Table III. These ΔE_x are then added to the predicted E_x of the remaining 1^+ levels of Table III in the calculation of the β^- decay phase space factors. The half-lifes calculated from the B(GT) of Table V are indicated for the three cases. The experimental half-life is 8.8(22) s (Ref. 11).

B. ^{40}S beta decay and the even-parity levels of ^{40}Cl

Four β^- delayed γ rays were assigned to ^{40}S decay by Dufour, *et al.*[11] Two possible placements of these γ transitions are shown in the bottom panel of Fig. 2. A 212-keV transition was also observed by Kozub, *et al.*[15] as was a weak 432-keV transition. The existence of an 889-keV level is practically certain since both crossover and cascade transitions can be assigned. We consider that two placements of the 432-keV transition are possible; hence a level at either 432 or 643 keV.

A further ambiguity is found in associating the $4fp$ level scheme of Table III with the experimental scheme. It appears quite likely that the 889-keV level is populated significantly by direct β^- decay and thus has $J^\pi=1^+$, as we indicate. However, as shown in the three schemes in the upper panel of Fig. 2, it could be either 1_1^+ or 1_2^+ (Ref. 26). For all three proposed schemes the major β^- branch is predicted to be a $\sim$44% branch to 1_4^+, and the branching to the 1^+ state(s) below 1 MeV is predicted to be 37%, 40%, and 14% for (a), (b), and (c), respectively. Thus we predict ample missing γ flux to make up the observed γ intensities out of the 212-keV level and the 643-keV level (if it is 2^+), i.e., we have predicted negligible direct β^- flux into the 1_1^- state and β^- decay to a 2^+ state would be second forbidden and thus negligible. That this flux is "missing" seems reasonable since the γ ray detection sensitivity of Dufour *et al.* fell off rapidly with energy and also the γ flux from higher-lying 1^+ states to the low-lying states below 1 MeV is predicted to be spread over many transitions and thus accordingly harder to detect.

All three schemes of Fig. 2 give reasonable agreement with the meager experimental facts. Schemes (a) and (b) do give better agreement with the half-life than (c). On the other hand, (c) does least damage to the even-parity level scheme of Table III, i.e., the predicted spacing of 869 keV between 1_1^+ and 1_2^+.

V. SUMMARY

Predictions have been given for binding energies, energy spectra, β^- decay, γ decay, and charge-exchange OBDME. The binding energy predictions for the ^{40}S and ^{40}Cl ground states are in good accord with experiment. The predicted odd-parity energy spectrum of ^{40}Cl is in excellent agreement with the most probable one of Kozub *et al.* The root-mean-square deviation for four levels [the three excited states for which Kozub *et al.* assigned probable spins (Fig. 1) and the 212-keV level (assumed 1_1^-)] is 95 keV. The present odd-parity ^{40}Cl level scheme is quite similar to that of Woods.[9] The differences are presumably due more to the differences in the interactions rather than in the model spaces. By contrast, the large differences in the excitation energies of 3_1^- and 2_2^- between our results and those of Ji and Wildenthal[10] are presumably mainly due to their use of a $d_{3/2}f_{7/2}$ model space. That is, we find the 3_1^- and 2_2^- states are only 47% and 30% $d_{3/2}^{-3}f_{7/2}^{3}$, respectively.

The complexity of the odd-parity ^{40}Cl wave functions is evident from an examination of the ^{40}Ar$\rightarrow^{40}$Cl charge-exchange reaction. This is especially true for the 2^- and 3^- states. Although a few general conclusions can be reached, understanding of the observed relative cross sections is not possible without a quantitative description of the reaction mechanism.

First-forbidden beta decay was calculated with complete *sdpf* bases for the ^{40}Cl levels and the ^{40}S ground state. We consider the results quite reliable. We find essentially negligible contribution to the total β^- decay.

The allowed (Gamow-Teller) decay was calculated with a highly truncated *sdpf* basis for the ^{40}Cl 1^+ states. Thus the gross properties—such as the summed B(GT) strength and the total half-life—are probably reliable, but not the details—such as the individual B(GT).

It is hoped that the predictions and comparison to experiment given here will help stimulate the further experimental work necessary for an understanding of these interesting neutron-rich nuclei.

ACKNOWLEDGMENTS

Research supported by the U.S. Department of Energy under Contract Nos. DE-AC02-76CH00016 (Brookhaven National Laboratory) and W-7405-Eng-48 with the University of California (Lawrence Livermore National Laboratory). One of us (E.K.W.) is grateful for an Alexander von Humboldt-Stifung which supported that part of the research carried out at the Max-Planck-Institut. We thank D. J. Millener for valuable discussions.

[1]E. K. Warburton, D. E. Alburger, J. A. Becker, B. A. Brown, and S. Raman, Phys. Rev. C **34**, 1031 (1986).
[2]E. K. Warburton and J. A. Becker, Phys. Rev. C **35**, 185 (1987).
[3]E. K. Warburton, Phys. Rev. C **35**, 2278 (1987).
[4]E. K. Warburton, J. A. Becker, D. J. Millener, and B. A. Brown, The WBMB Shell-Model Interaction and the Structure of ^{16}O(2s,1d)$^{A-16-n}$(1f,2p)^n Levels in A=31-44 Nuclei with Particular Emphasis on Binding Energies and Energy Spectra, BNL Report No. 40890, 1987 (unpublished).
[5]E. K. Warburton and J. A. Becker, Phys. Rev. C **37**, 754 (1988).
[6]D. E. Alburger and E. K. Warburton, Phys. Rev. C **38**, 1843 (1988).
[7]E. K. Warburton, J. A. Becker, B. A. Brown, and D. J. Millener, Ann. Phys. (N.Y.) **187**, 471 (1988).
[8]E. K. Warburton and D. E. Alburger, Phys. Rev. C **38**, 2822 (1988).
[9]C. L. Woods, Nucl. Phys. **A451**, 413 (1986).
[10]X. Ji and B. H. Wildenthal, Phys. Rev. C (to be published).
[11]J. P. Dufour, R. Del Morak, A. Fleury, F. Hubert, D. Jean, M. S. Pravikoff, H. Delagrange, H. Geissel, and K. H. Schmidt, Z. Phys. A **324**, 487 (1986).
[12]P. M. Endt and C. Van der Leun, Nucl. Phys. **A310**, 1 (1978).

[13]A. Huck, G. Klotz, A. Knipper, C. Miehe, C. Richard-Serre, and G. Walter, in Proceedings of Fourth International Conference on Nuclei Far from Stability, edited by P. G. Hansen and O. B. Nielsen, CERN, Geneva, 1981 (unpublished).

[14]L. K. Fifeld, M. A. C. Kotchkis, P. V. Drumm, T. R. Ophel, G. D. Putt, and D. C. Weisser, Nucl. Phys. **A417**, 534 (1984).

[15]R. L. Kozub, J. F. Shriner, Jr., M. M. Hindi, R. Holzmann, R. V. F. Janssens, T. L. Khoo, W. C. Ma, M. Drigert, U. Garg, and J. J. Kolata, Phys. Rev. C **37**, 1791 (1988).

[16]B. H. Wildenthal, Prog. Part. Nucl. Phys. **11**, 5 (1984).

[17]J. P. McGrory, Phys. Rev. C **8**, 693 (1973).

[18]D. J. Millener and D. Kurath, Nucl. Phys. **A255**, 315 (1975).

[19]B. A. Brown, A. Etchegoyen, W. D. M. Rae, and N. S. Godwin, OXBASH, 1984 (unpublished).

[20]D. H. Gloeckner and R. D. Lawson, Phys. Lett. **53B**, 313 (1974).

[21]A. H. Wapstra and G. Audi, Nucl. Phys. **A432**, 1 (1985).

[22]B. A. Brown and B. H. Wildenthal, At. Data Nucl. Tables **33**, 347 (1985).

[23]B. A. Brown and B. H. Wildenthal, Nucl. Phys. **A474**, 2990 (1987).

[24]I. S. Towner, Phys. Rep. **155**, 264 (1987).

[25]Experimentalists will immediately recognize the difficulty of observing a 595-keV γ ray with Ge γ detectors.

[26]There are, of course, other possibilities. For instance, there is no certainty that the 212-keV level has odd parity. The schemes of Fig. 2 are our subjective estimate as to the most probable ones.